Hindawi Publishing Corporation
Advances in Materials Science and Engineering
Volume 2015, Article ID 727141, 14 pages
http://dx.doi.org/10.1155/2015/727141

*Research Article*

# Experimental Investigation on Mechanical and Turning Behavior of Al 7075/*x*%wt. $TiB_2$-1% Gr In Situ Hybrid Composite

**K. R. Ramkumar, Habtamu Bekele, and S. Sivasankaran**

*School of Mechanical and Electromechanical Engineering, Institute of Technology, Hawassa University, Awasa 1530, Ethiopia*

Correspondence should be addressed to S. Sivasankaran; sivasankarangs1979@gmail.com

Received 17 August 2015; Accepted 12 November 2015

Academic Editor: Filippo Giannazzo



The present research work involves the study of AA 7075-$TiB_2$-Gr in situ composite through stir casting route. This in situ method involves formation of reinforcements within the matrix by the chemical reaction of two or more compounds which also produces some changes in the matrix material within the vicinity. Titanium Diboride ($TiB_2$) and graphite were the reinforcement in a matrix of AA 7075 alloy. The composite was prepared with the formation of the reinforcement inside the molten matrix by adding salts of Potassium Tetrafluoroborate ($KBF_4$) and Potassium Hexafluorotitanate ($K_2TiF_6$). The samples were taken under casted condition and the properties of the composite were tested by conducting characterization using X-ray diffraction (XRD), hardness test, flexural strength by using three-point bend test, scanning electron microscope (SEM), optical microstructure, grain size analysis, and surface roughness. It was found that good/excellent mechanical properties were obtained in AA 7075-$TiB_2$-Gr reinforced in situ hybrid composite compared to alloy due to particulate strengthening of ceramic particles of $TiB_2$in the matrix. Further, Al 7075-3% $TiB_2$-1% Gr hybrid in situ composite exhibited improved machinability over the alloy and composites due to self-lubricating property given by the Gr particles in the materials.

## 1. Introduction

Composite material is composed of two or more materials at a microscopic scale and has chemically distinct phases. In ordinary conventional materials the required properties cannot be obtained. However by using the composite materials the needed properties in the required materials can easily be achieved. In metal matrix composites (MMCs) high strength and fracture toughness and stiffness are offered by metal matrices compared to those offered by their polymer counterparts [1–5]. They can withstand elevated temperature in corrosive environment compared to polymer composites [6]. Aluminium based particulate reinforced MMCs have emerged as an important class of high performance and it has low density and high thermal conductivity [7]. To improve its strength, high elastic modulus, and increased wear resistance over conventional base alloys, AA 7075 alloy was selected because of its low specific weight and high strength-to-weight ratio and also its excellent machinability, formability, and weldability [8]. This alloy is widely used in automotive industry, aircraft industry, and defense industries [9, 10]. The composite was prepared with the formation of the reinforcement inside the molten matrix of Titanium Diboride ($TiB_2$) which was obtained by adding salts of Potassium Tetrafluoroborate ($KBF_4$) and Potassium Hexafluorotitanate ($K_2TiF_6$) [11]. $TiB_2$ is well known as a ceramic material with relatively high strength and durability as characterized by the relatively high values of its melting point, hardness, strength-to-density ratio, and wear resistance [9].

In the in situ methods reinforcements are clean and thermodynamically stable. This method gives better mechanical properties due to the effective bonding between the matrix and the reinforcements. This method is especially for the metal matrix composite [12]. Reinforcements are added in the form of salts. These salts react inside the molten matrix to form the reinforcements. In situ techniques lead to

Table 1: Chemical composition of AA 7075 alloy.

| Elements | Si | Fe | Cu | Mg | Zn | Ti | Cr | Al |
|---|---|---|---|---|---|---|---|---|
| wt.% | 0.2 | 0.23 | 1.71 | 2.46 | 5.29 | 0.54 | 0.21 | Bal. |

Table 2: Amount of chemical salts required for formation of $TiB_2$.

| % | Al (7075) alloy, in Kg. | $TiB_2$, in gm. | |
|---|---|---|---|
| | | $K_2TiF_6$, in gm. | $KBF_4$, in gm. |
| 0 | 1 | 0 | 0 |
| 1.5 | 1 | 21.46 | 22.54 |
| 3 | 1 | 42.93 | 45.09 |
| 4.5 | 1 | 64.39 | 67.63 |
| 6 | 1 | 85.86 | 90.12 |

better adhesion at the interface and hence better mechanical properties [13]. The composite material can be made by different types of processes but here most commercially used technique of stir casting method was selected because of its most potential method for engineering applications in terms of production capacity and cost efficiency [14]. The technology is relatively simple and of low cost. Based on several literatures, there is no work related to Al 7075-$Tib_2$-Gr in situ hybrid composite on mechanical and turning behavior. Therefore, the present work carried out the detailed study and investigation on microstructure and mechanical and turning behavior of Al 7075-$TiB_2$-Gr in situ hybrid composite.

## 2. Materials and Methods

*2.1. Material Choice.* In this study, AA 7075 alloy (Al-Zn-Mg-Cu-Si-Mn-Fe-Mn-Ti-Cr) had been chosen because it has excellent machinability and formability and low specific weight and high strength-to-weight ratio compared to many other aluminium alloys [4]. The chemical composition of AA 7075 is shown in Table 1. Tests for the results (Table 1) were carried out as per optical emission spectrophotometer (OSM) in order to conform the matrix.

*2.2. Manufacturing of AA 7075-$TiB_2$-Gr Reinforced In Situ Hybrid Composite.* AA 7075/$x$% $TiB_2$-1% Gr ($x$ = 0, 1.5, 3, 4.5, and 6 wt.%) were prepared by the addition of Potassium Hexafluorotitanate ($K_2TiF_6$) and Potassium Tetrafluoroborate ($KBF_4$). The chemical reaction is a multistage reaction. The compound reaction is shown in

$$3K_2TiF_6 + 6KBF_4 + 22Al \longrightarrow 3TiB_2 + 12Al + \left(9KAlF_6 + K_3AlF_6\right) \quad (1)$$

The addition of salts based on sample composition for getting different samples is given in Table 2.

This work involves the manufacturing of composite material of Al 7075/$x$% $TiB_2$-Gr hybrid composites by stir casting technique (Figure 1(a)). In this method, the Al 7075 is initially kept in a crucible furnace and it is heated to a temperature of 760°C. Then the powers of $K_2TiF_6$ and $KBF_4$ are mixed finely through stirring to achieve $TiB_2$. Then it is preheated to a temperature of 200°C. In the meantime, the Al 7075 attained its liquid state and the stirring motor was switched on. The stir casting set-up consists of a blade which was made of graphite coated stainless steel. The speed of the stirrer was limited to 300 rpm. After reaching the vortex in the molten metal, the preheated chemical salts with size of 200 $\mu$m were mixed evenly. During the mixing the stirrer rotates at a constant speed. Then the mixed molten metal was kept out for some time (10 min) at high temperature for the chemical reaction to take place, due to which the reinforcement will form in the molten metal. After completing the chemical reactions, the 1% of graphite was added to the molten metal and mixed properly. Finally the molten metal was poured in the circular die of the size 30 mm diameter and 250 mm length.

*2.3. Characterization Technique.* X-ray diffraction (XRD) (using Cu-K$\alpha$ radiation and operating at 40 kV and 100 mA) method was carried out to confirm the phases in fabricated hybrid composites. Those which require high magnification to be visible are termed microstructures. Microscopes are required for the examination of the microstructure of the metals. The maximum possible magnification with an electron microscope is approximately 2000 diameters. Then, the surface to be examined is scanned with an electron beam, and the reflected beam of electrons is collected and then displayed at the same scanning rate on a cathode ray tube. Magnifications ranging from 10 to an excess of 50 000 diameters and also very great depths of field are possible. Therefore, optical microscopes and scanning electron microscopes were used to examine the microstructures of the fabricated hybrid composites [5]. Finally the microtexture of inserts before and after turning has been analyzed at highest cutting parameters and flank wear, nose deformation, and erosion of material over the tool have been examined.

*2.4. Turning Process.* The turning experiments were carried out on Smart Jr CNC Turning centre using TiN coated carbide insert (K10) (Figure 1(b)). The cutting speed was selected (based on commercial one) in a range of 180 mm/min to 240 mm/min, feed rate range was selected in the range of 0.1 mm/rev to 0.3 mm/rev, depth of cut was selected in a range of 0.5 mm to 1.5 mm, and the surface roughness has been done by using 0.4 mm and 0.8 mm nose radius insert. Three types of combinations of feed rate and depth of cut were chosen in order to measure the surface roughness of the machined product.

*2.5. Mechanical Property Measurement.* Hardness tests were used to determine the strength of a material to judge deformation ability. A standard specimen of 6.4 mm thickness is cut from fabricated composites. The material hardness was tested based on the standard of IS: 1500-205 of "B" scale. The given load is 100 Kgf and ball size is 1.5875 mm (indenter). Flexural strength has been obtained by conducting three-point bending test (Figure 1(c)) which is made up of D3 steel. The D3 steel contains high carbon and high chromium. The samples are machined as per standards and then we heat treated it by hardening and ageing. Finally it was

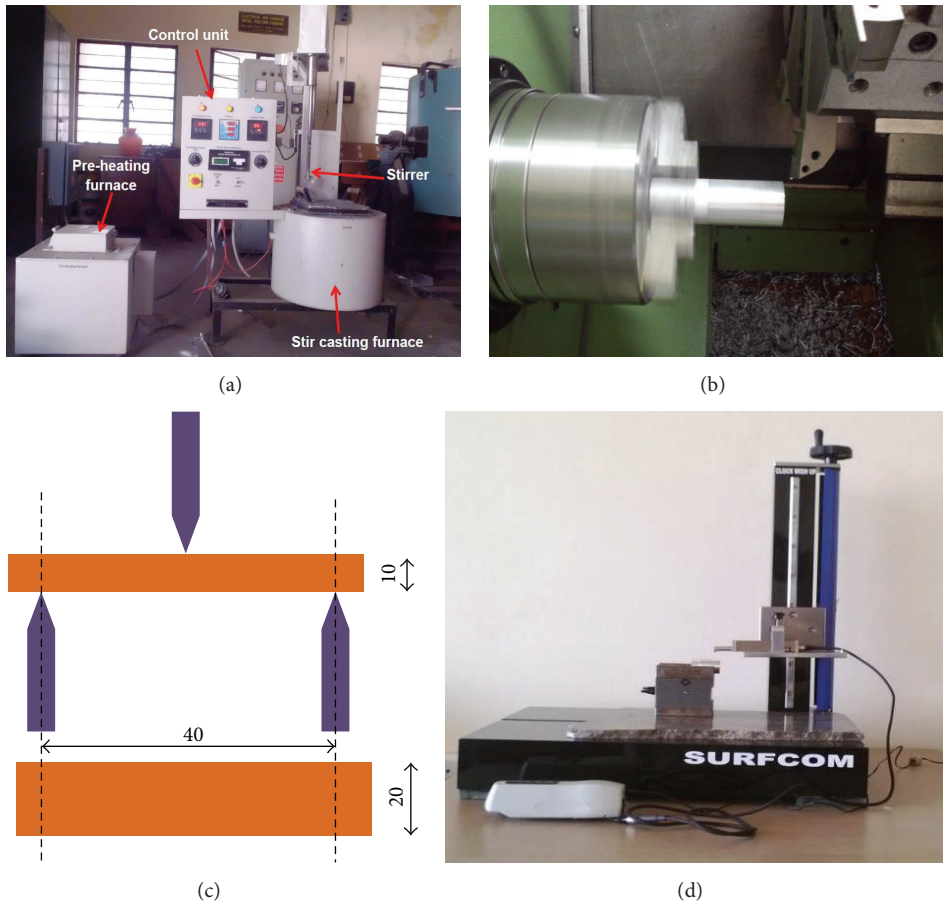


FIGURE 1: (a) Stir casting set-up. (b) Smart Jr CNC Turning centre. (c) Schematic of three-point bending test. (d) Handysurf surface roughness measuring device.

grinded to improve the surface finish. The flexural strength is used to determine the bending stress and deflection and flexural stain. The flexural test was carried out with crosshead movement of 1 mm per minute. Three samples were taken from each composition and the mean values were used for investigation. The schematic of three-point bending test is shown in Figure 1(c). The Handy Surf E-DTS5706 was used to measure the surface roughness. It consists of a probe which records the surface roughness using a 4 mN of measuring force and a 5 $\mu$m radius diamond end, 90° cone measuring probe. The set-up is shown in Figure 1(d).

## 3. Results and Discussion

*3.1. Examination of Hardness Test.* The hardness behavior of fabricated both hybrid and monocomposite is shown in Figure 2. From Figure 2(a), it is revealed that the strength of hybrid composite started to increase steadily up to 3% $TiB_2$ and then increases slowly. This was due to more formation of $TiB_2$ particles which imported particulate strengthening in the matrix. The strength of Al 7075-3% $TiB_2$-1% Gr hybrid composite exhibited 25% more than Al 7075-0% $TiB_2$-1% Gr monocomposite. However, the strength of Al 7075-6% $TiB_2$-1% Gr hybrid composite exhibited only 3.8% more than Al 7075-3% $TiB_2$-1% Gr hybrid composite and 29% higher than Al 7075-0% $TiB_2$-1% Gr monocomposite. Therefore, it was decided to stop the addition of reinforcement formation up to 6% $TiB_2$ particles. Further, the strength of Al 7075-3% $TiB_2$ (Figure 2(b)) monocomposite produced only 3.5% higher than Al 7075 alloy. Hence, the examination towards the addition of reinforcement to formation of $TiB_2$ particle beyond 3% in monocomposite was not carried out. Based on the results obtained from Figure 2, it can be concluded that the hybrid composite of Al 7075-3% $TiB_2$-1% Gr showed improvement in hardness compared to others.

*3.2. Evaluation of Flexural Strength.* The observed value of bending stress and deflection and flexural strain of Al 7075 + $x$% $TiB_2$ + 1% Gr hybrid composites ($x$ = 0, 1.5, 3, 4.5, and 6) (Figures 3(a), 3(c), and 3(d)) and the bending stress of monocomposite (Figure 3(b)) are shown in Figure 3. From Figures 3(a), 3(c), and 3(d), with increasing the amount of reinforcement, the bending stress and deflection and flexural strain value are increased up to 3% $TiB_2$/1% Gr reinforcement. This was attributed to the presence of hard ceramic particles and graphite particles. Further, it was expected to form uniform embedding of $TiB_2$ particles over the matrix. However, the bending stress and deflection and flexural strain were started

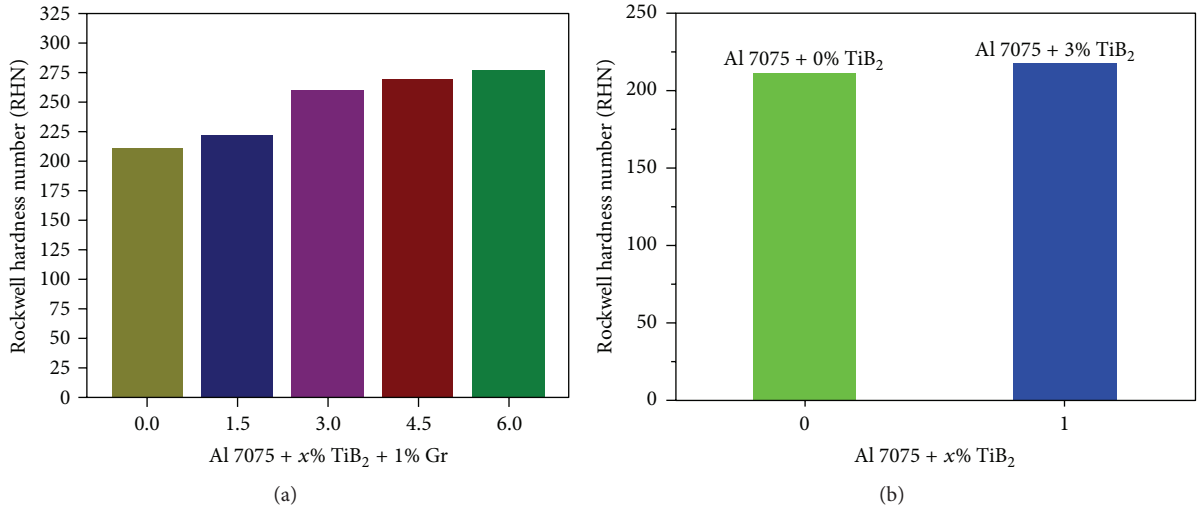


Figure 2: Rockwell hardness number for (a) Al 7075 + $x$% $TiB_2$ + 1% Gr hybrid composites ($x$ = 0, 1.5, 3, 4.5, and 6) and (b) Al 7075 + $x$% $TiB_2$ monocomposite ($x$ = 0 and 3).

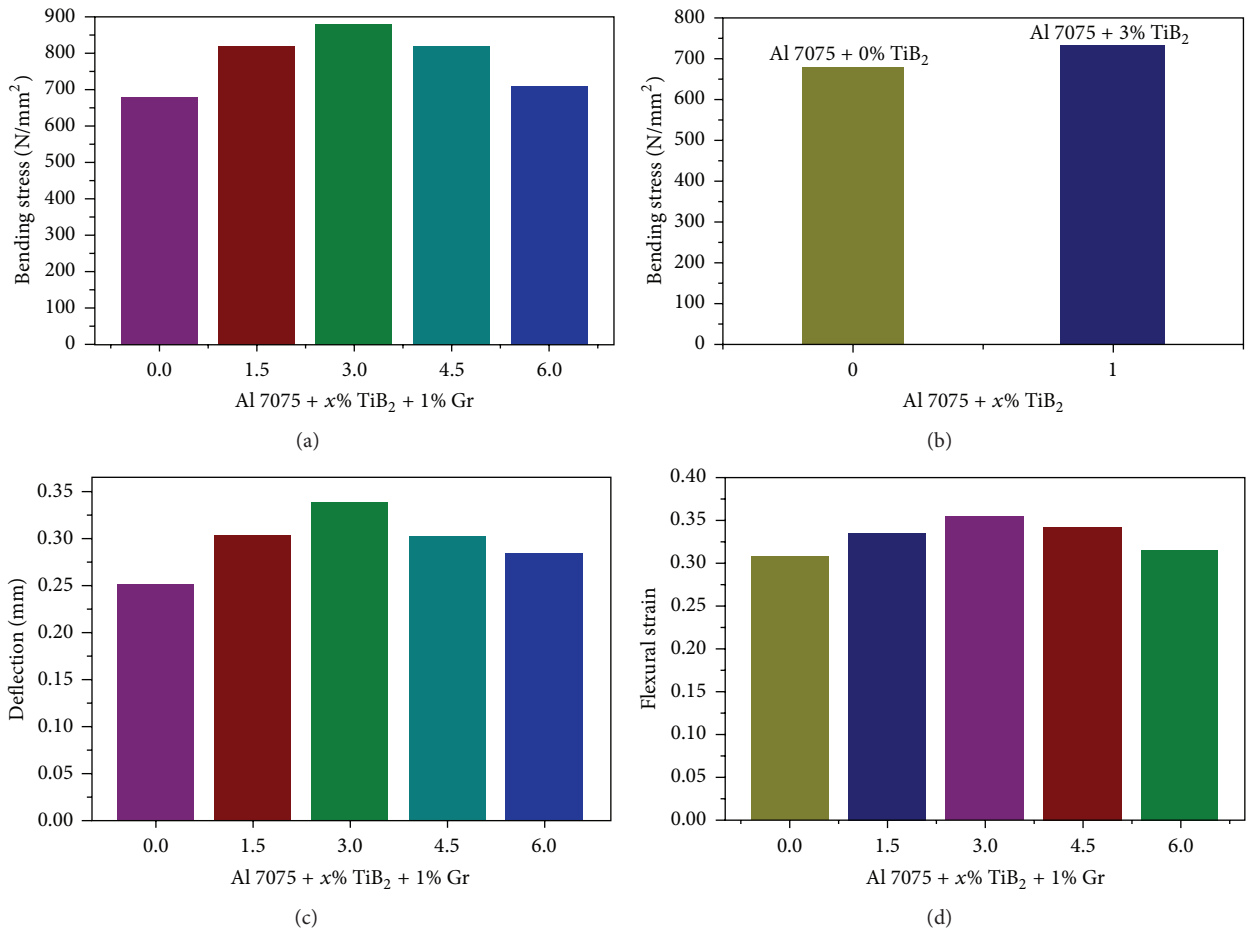


Figure 3: Bending stress for (a) Al 7075 + $x$% $TiB_2$ + 1% Gr hybrid composites ($x$ = 0, 1.5, 3, 4.5, and 6), (b) Al 7075 + $x$% $TiB_2$ monocomposite ($x$ = 0 and 3), (c) deflection for Al 7075 + $x$% $TiB_2$ + 1% Gr hybrid composites ($x$ = 0, 1.5, 3, 4.5, and 6), and (d) flexural strain for Al 7075 + $x$% $TiB_2$ + 1% Gr hybrid composites ($x$ = 0, 1.5, 3, 4.5, and 6).

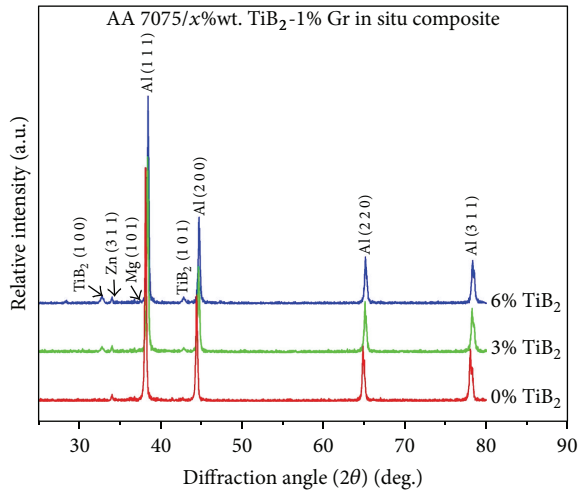


FIGURE 4: XRD results of Al 7075 + $x$% $TiB_2$ + 1% Gr hybrid composites ($x$ = 0, 3, and 6).

to decrease beyond 3% $TiB_2$ in situ composites. This was expected to nonuniform embedded $TiB_2$ particles along with its agglomeration over the matrix. Further, the bending stress of monocomposite (Figure 3(b)) is lower than that of hybrid composite (Figure 3(a)). The bending stress of monocomposite (3%) was around 8.8% higher than monolithic alloy. However, the hybrid composite of Al 7075 + 3% $TiB_2$ + 1% Gr sample exhibited around 30% higher than monolithic alloy, 19% higher than 3% monocomposite, and 22% higher than 6% hybrid composite. These results also showed that the hybrid composite of Al 7075 + 3% $TiB_2$ + 1% Gr produced excellent results when compared to other samples. This was expected due to uniform distribution/embedding of 3% $TiB_2$ particles and 1% Gr particles.

*3.3. Examination of X-Ray Diffraction Analysis and Optical Microstructural Analysis.* The X-ray diffraction profile analysis of prepared hybrid composite is shown in Figure 4. From Figure 4, the diffraction peaks of $TiB_2$ particles were observed clearly and the peaks increase as $TiB_2$ chemical salts content was increased which indicated the increasing of the amount of formation of $TiB_2$ particles over the matrix. From the XRD analysis, the presence of $TiB_2$ particles and Gr was conformed in AA 7075 matrix alloy. The Al 7075 peaks were higher because of larger amount of matrix materials present in the fabricated composites. It was observed that there was no $TiB_2$ peak formation at 0%, while increasing the amount of $TiB_2$ chemical salts the peak also increased. 6% of $TiB_2$ peaks were higher than the 3% of $TiB_2$; this indicates that the in situ formed $TiB_2$ particles were thermodynamically stable and the interface between aluminum alloy and $TiB_2$ particles tends to be free. There was no graphite peak for 1% graphite added sample because the XRD can show only if the amount of any constituent is more than 2%.

The optical micrographs of the hybrid composite of Al 7075/$x$% wt. $TiB_2$/1% Gr ($x$ = 0, 1.5, 3, 4.5, and 6% wt.) are shown in Figures 5(a)–5(f). Common casting defects such as porosity, shrinkages, or slag inclusion were present in Figure 5(a) and the matrix had large size of grains. While considering Figure 5(b), these defects are decreased due to presence of 1.5% $TiB_2$ + 1% Gr reinforcements. But the amounts of reinforcements were comparatively low and little amount of grain size starts to decrease. The dark color particles were corresponding to $TiB_2$ particles and the big grey colour particles were corresponding to Gr. It was observed that the amount of formed $TiB_2$ particles started to increase corresponding to the increasing of chemical salts. Hence, the formation of $TiB_2$ particles was conformed and visually observed from microstructures (Figure 5). Figures 5(c) and 5(f) show the presence of 3% $TiB_2$ particles. This picture shows good bonding strength and uniform distribution of reinforcement in the matrix. However, the formation of agglomeration/nonuniform distributed formed $TiB_2$ particles can be observed from Figure 5(e) which might have decreased the mechanical properties when the formation of reinforcement goes beyond 3%. Further, the grain size of Al 7075/$x$% wt. $TiB_2$/1% Gr ($x$ = 0, 1.5, 3, 4.5, and 6% wt.) is shown in Figure 6. Grain size of 0% reinforcement material shows more size, so it results in possessing of lower strength. While increasing the formation of reinforcement percentages to 1.5, 3, 4.5, and 6% with 1% Gr there was a considerable decrease in the grain size considerably up to 3% and then it started to decrease slowly up to 6%.

*3.4. Evaluation of Scanning Electron Microscopy (SEM) on Fabricated Hybrid Composite.* The SEM micrographs of the fabricated hybrid composite are presented in Figure 7. General casting defects such as porosity, cracks, and peel-off were seen in the Al 7075/0% $TiB_2$ composites. While adding the chemical salts for formation of 3% and 6% $TiB_2$/1% Gr reinforced hybrid composite, the in situ formed 3% $TiB_2$ particles were distributed nearly homogeneously in the matrix (Figure 7(b)) compared to 6% $TiB_2$ particulate hybrid composite (Figure 7(c)). Such kind of particulate distribution is an essential requirement to achieve enhanced mechanical properties of aluminium based hybrid composites. The in situ formed $TiB_2$ particles and graphite exhibit various shapes such as spherical, hexagonal, and cubic shapes. It was evident from Figures 7(b) and 7(c) that the interface between the $TiB_2$ and graphite particles and the matrix was clear and $TiB_2$ particles were well bonded to aluminum matrix. The presence of clear interface can be attributed to the thermodynamic stability of the $TiB_2$ particles and the formation of particles within the melt itself. When a ceramic particle behaves thermodynamically unstable in the aluminum melt, it produces undesirable compounds at the particle to matrix interface. A pure interface was needed to increase the load bearing capability of the aluminium matrix composites. In general, the increase in local melt temperature due to the in situ reaction causes good bonding between the $TiB_2$ particle, graphite, and the matrix which was achieved through the present research work. The corresponding EDAX analysis for 6% $TiB_2$/1% Gr composite is also shown in Figure 7(d) which conforms the presence of reinforcements and no intermetallic compounds were observed.

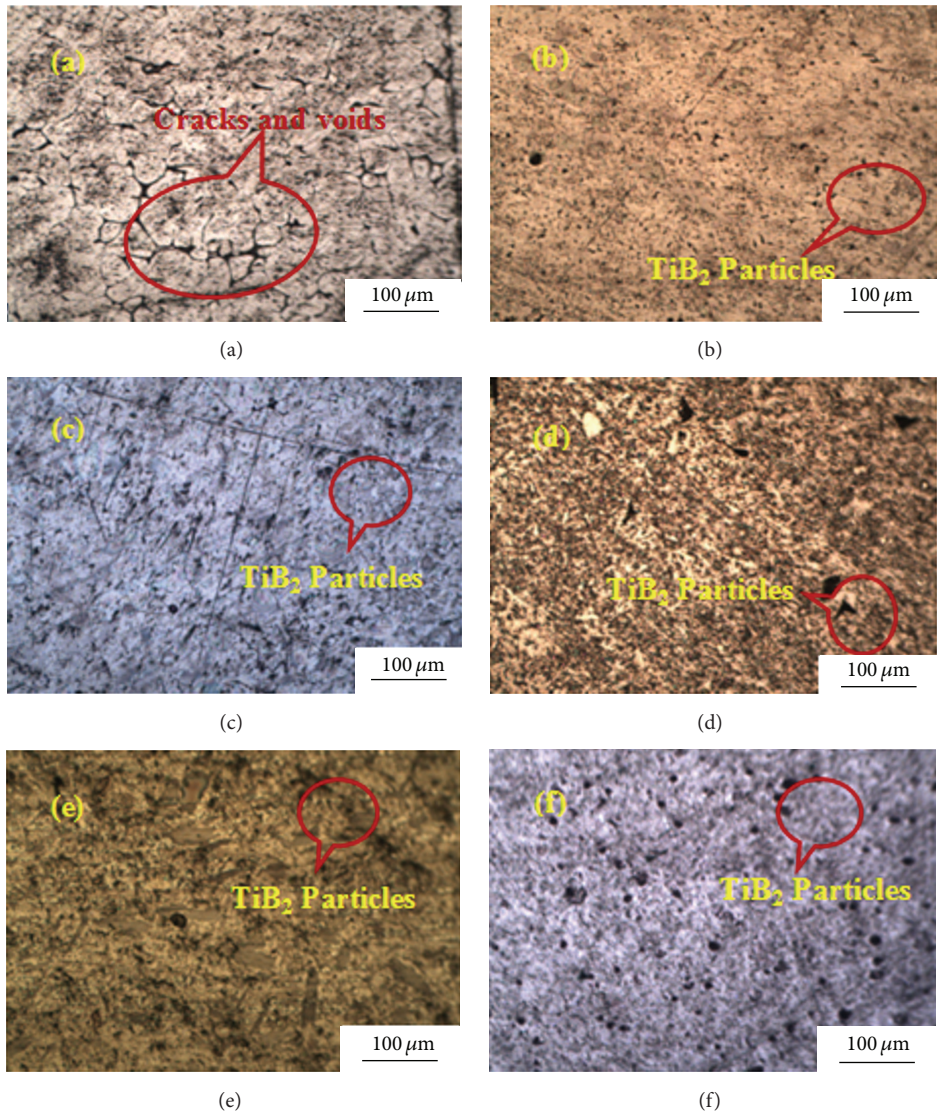


Figure 5: Microstructure images of Al 7075/$TiB_2$/Gr hybrid composites: (a) Al 7075/0% wt. $TiB_2$/1% Gr, (b) Al 7075/1.5% wt. $TiB_2$/1% Gr, (c) Al 7075/3% wt. $TiB_2$/1% Gr, (d) Al 7075/4.5% wt. $TiB_2$/1% Gr, (e) Al 7075/6% wt. $TiB_2$/1% Gr, and (f) Al 7075/3% wt. $TiB_2$.

The fractography images of three-point bend tested samples are shown in Figure 8. With this evaluation of fractography images in SEM analysis as shown in Figure 8, Al 7075-0% reinforcement samples (Figure 8(a)) have more dimples and crack propagation and also it was more ductile in nature. While adding the chemical salts for the formation of 3% $TiB_2$-1% Gr (Figure 8(b)) reinforcements to the Al 7075 matrix, it produced less dimples formation and it had good interfacial bonding in between matrix and reinforcements. These hybrid composite materials had changed the small amount ductile nature into brittle nature due to presence of hard ceramic particles. However, 6% $TiB_2$-1% Gr hybrid composite had produced more particulate crack and it had larger amount of brittle nature and hence it exhibited decrease in mechanical properties. This was due to presence of more amounts of hard ceramic particles in the Al 7075 matrix material and agglomeration of $TiB_2$ particles over the matrix.

*3.5. Evaluation of Turning Behavior in terms of Surface Roughness.* The values of surface roughness at different cutting speeds, feed rates, and depth of cuts while turning of Al 7075 + 0% reinforcement, Al 7075 + 3% $TiB_2$ + 1% Gr, and Al 7075 + 3% $TiB_2$ composites, respectively, using carbide insert with 0.4 mm and 0.8 mm nose radius are shown in Table 3 and Figure 9. Surface roughness of all fabricated composite material decreases by increasing the cutting speed from 180 to 240 m/min at the feed rate of 0.3 mm/rev. Similarly while increasing the feed rate and depth of cut values, the surface roughness values start to increase, and this would be controlled by increasing the cutting speed and also each condition of depth of cut, feed rate, the surface roughness decreases with increasing of cutting speed from 180 m/min to 240 m/min, while compared Al 7075 + 3% $TiB_2$ + 1% Gr composites produce lower value of surface roughness among all other composite with insert of both 0.4 mm and 0.8 mm

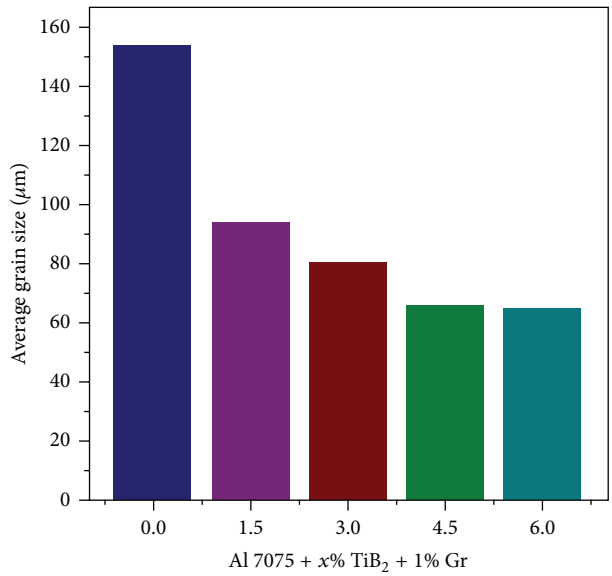


FIGURE 6: Grain size of Al 7075/$x$% $TiB_2$/1% Gr hybrid composites.

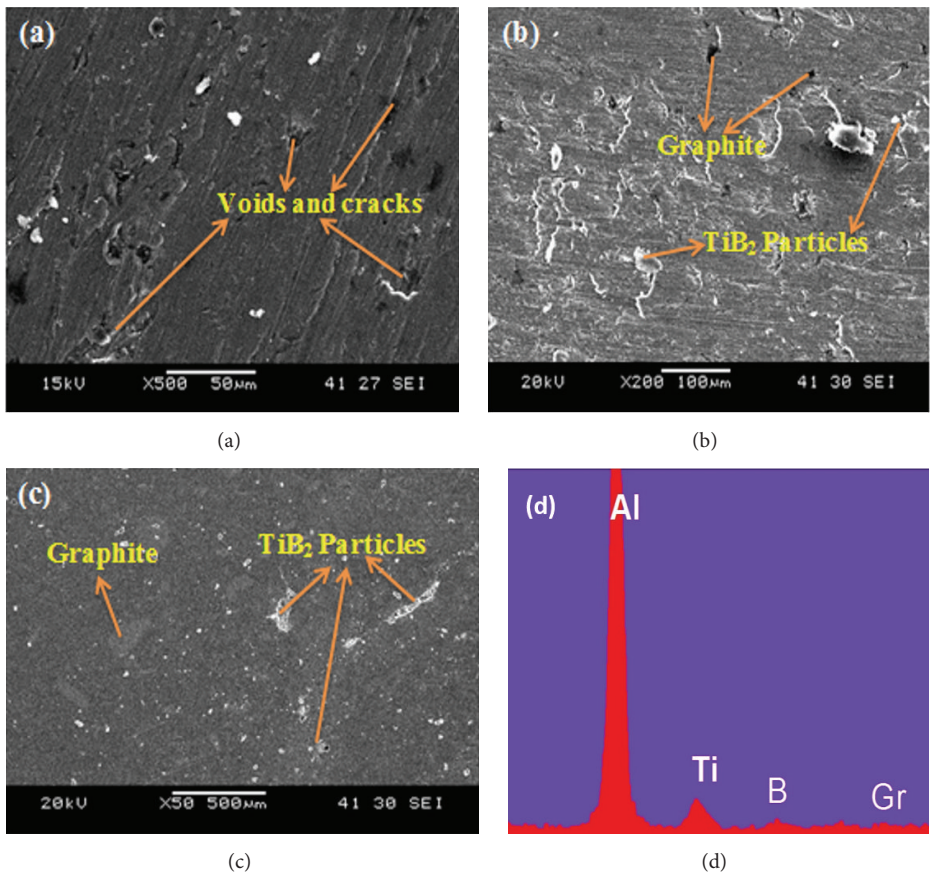


FIGURE 7: SEM images of Al 7075/$TiB_2$/Gr hybrid composites: (a) Al 7075/0% wt. $TiB_2$/1% Gr, (b) Al 7075/3% wt. $TiB_2$/1% Gr, (c) Al 7075/6% wt. $TiB_2$/1% Gr, and (d) sum spectrum produced by EDAX.

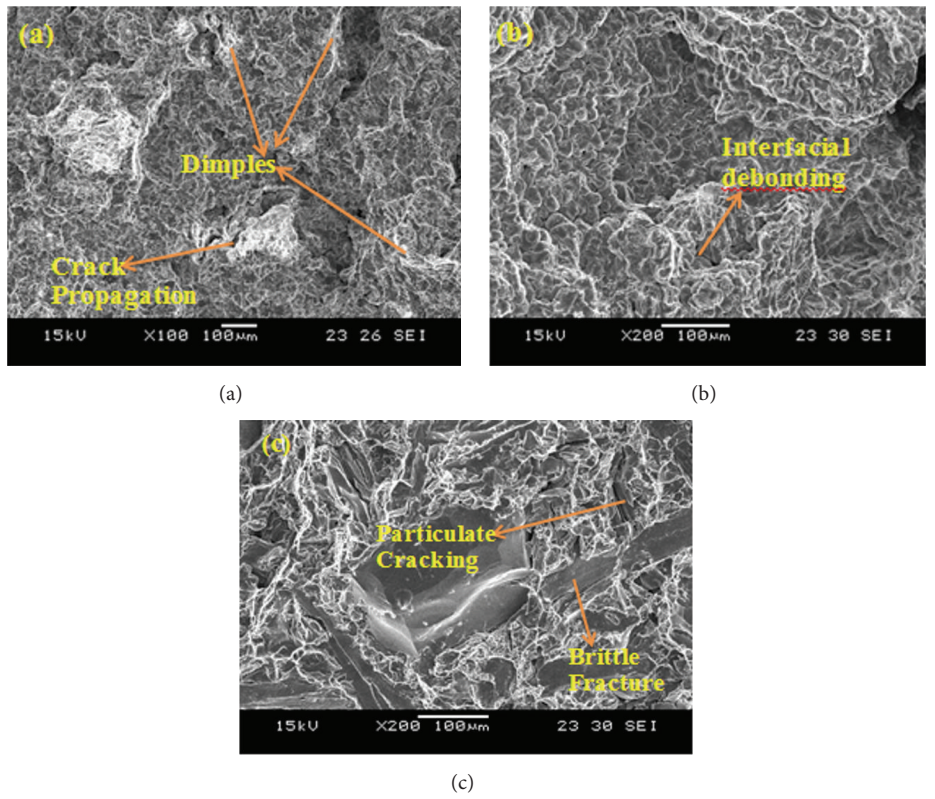


Figure 8: SEM fractography images of Al 7075/$TiB_2$/Gr hybrid composites: (a) Al 7075/0% wt. $TiB_2$/1% Gr, (b) Al 7075/3% wt. $TiB_2$/1% Gr, and (c) Al 7075/6% wt. $TiB_2$/1% Gr.

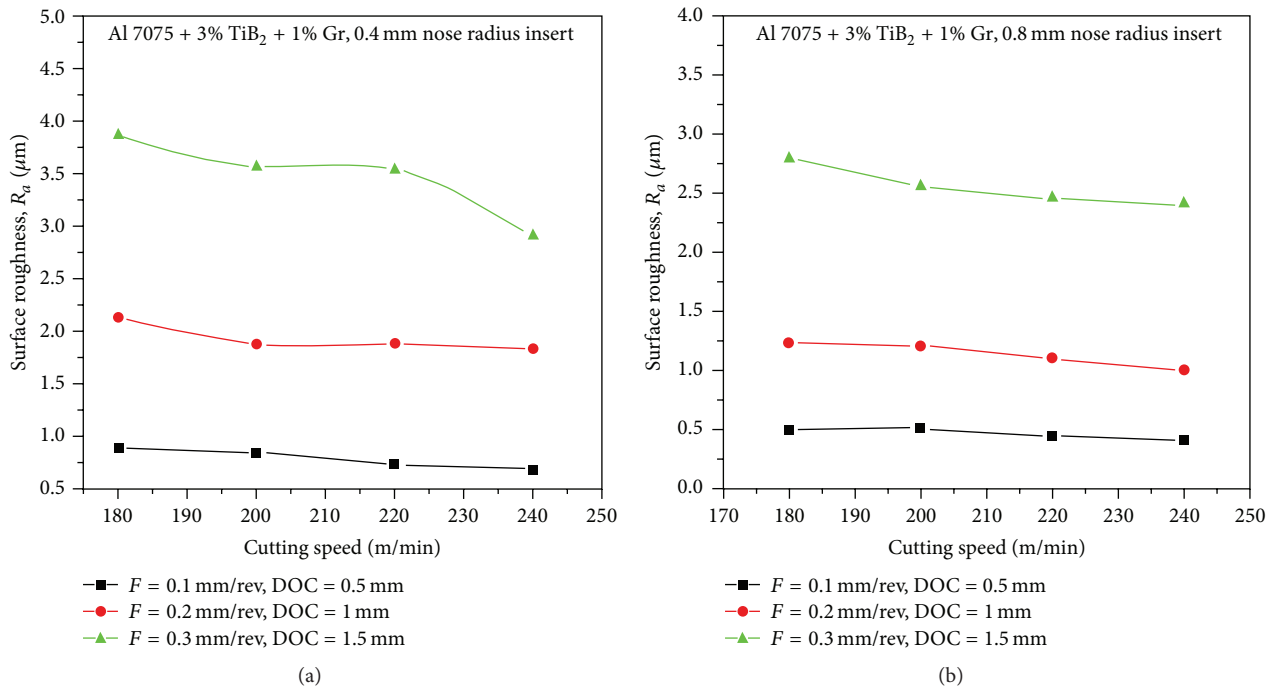


Figure 9: Variations of surface roughness on 0.4 mm and 0.8 mm nose radius of Al 7075 + 3% $TiB_2$-1% Gr composites.

Table 3: Experimental values of surface roughness by using 0.4 mm and 0.8 mm nose radius inserts.

| Material | Feed (mm/rev) | Depth of cut (mm) | Cutting speed (m/min) | Average surface roughness ($R_a$, in $\mu$m) | |
|---|---|---|---|---|---|
| | | | | 0.4 mm nose radius insert | 0.8 mm nose radius insert |
| Al 7075 + 0% $TiB_2$ + 1% Gr | 0.1 | 0.5 | 180 | 0.948 | **0.358** |
| | | | 200 | 0.810 | **0.343** |
| | | | 220 | 0.740 | **0.319** |
| | | | 240 | 0.671 | **0.289** |
| | 0.2 | 1.0 | 180 | 2.570 | **1.310** |
| | | | 200 | 2.353 | **1.290** |
| | | | 220 | 2.289 | **1.100** |
| | | | 240 | 2.156 | **1.039** |
| | 0.3 | 1.5 | 180 | 3.754 | **2.756** |
| | | | 200 | 3.662 | **2.711** |
| | | | 220 | 3.461 | **2.661** |
| | | | 240 | 3.111 | **2.558** |
| Al 7075 + 3% $TiB_2$+ 1% Gr | 0.1 | 0.5 | 180 | 0.882 | **0.507** |
| | | | 200 | 0.843 | **0.519** |
| | | | 220 | 0.736 | **0.456** |
| | | | 240 | 0.680 | **0.416** |
| | 0.2 | 1.0 | 180 | 2.134 | **1.240** |
| | | | 200 | 1.882 | **1.211** |
| | | | 220 | 1.877 | **1.111** |
| | | | 240 | 1.836 | **1.011** |
| | 0.3 | 1.5 | 180 | 3.875 | **2.809** |
| | | | 200 | 3.575 | **2.572** |
| | | | 220 | 3.545 | **2.473** |
| | | | 240 | 2.911 | **2.412** |
| Al 7075 + 3% $TiB_2$ | 0.1 | 0.5 | 180 | 1.117 | **0.761** |
| | | | 200 | 1.081 | **0.740** |
| | | | 220 | 1.011 | **0.685** |
| | | | 240 | 0.949 | **0.598** |
| | 0.2 | 1.0 | 180 | 2.657 | **1.318** |
| | | | 200 | 1.863 | **1.291** |
| | | | 220 | 1.751 | **1.210** |
| | | | 240 | 1.711 | **1.171** |
| | 0.3 | 1.5 | 180 | 3.692 | **2.238** |
| | | | 200 | 3.458 | **2.195** |
| | | | 220 | 3.342 | **2.115** |
| | | | 240 | 3.128 | **2.095** |

nose radius. So, Al 7075 + 3% $TiB_2$ + 1% Gr composites produce better surface finish, due to present soft graphite particles. Finally, the surface roughness was compared to 0.4 mm nose radius insert and 0.8 mm nose radius insert for all fabricated composites. The 0.8 mm nose radius insert produces lower value of surface roughness. The reason was expected due to that the contact between the tool and workpiece was more in 0.8 mm nose radius insert and also reduces the tool wear and tool breakdown while increasing value of feed rate and depth of cut values during turning process. Due to above reason tool life and surface finish would be increased in 0.8 mm nose radius insert.

The chip morphology of Al 7075 monolithic alloy, Al 7075-0% $TiB_2$-1% Gr monocomposite, Al-7075-3% $TiB_2$-0% Gr monocomposite, and Al 7075-3% $TiB_2$-1% Gr hybrid composites turned by using 0.4 mm and 0.8 mm nose radius is shown from Figures 10–13. A very thin almost continuous chip was observed in graphite reinforced alloy (right of Figure 10). The lower amount of continuous chips was observed in Al 7075-3% $TiB_2$ in situ composite (left of

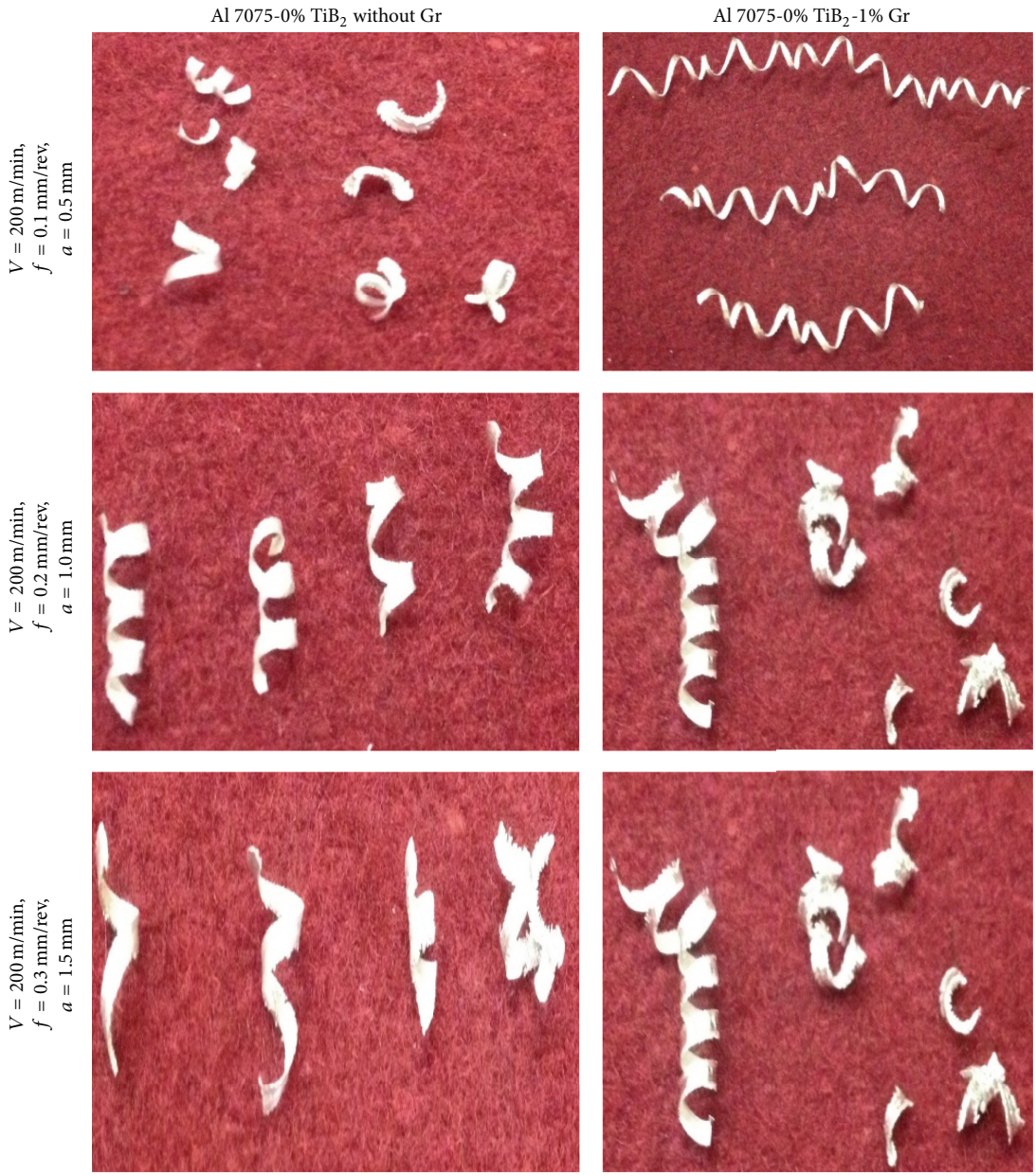


FIGURE 10: Examination of chip morphology with selected cutting parameters of AA 7075-3% $TiB_2$-0% Gr and AA 7075-3% $TiB_2$-1% Gr hybrid in situ composite with the cutting tool of 0.8 nose radius insert.

Figure 11) and a discontinuous chip was observed in graphite reinforced composite (right of Figure 12). Further, for the high rate of feed, depth of cut, and cutting speed, less damage surface (serrations) was observed in the case of graphite reinforced alloy and composite. This was attributed to acicular structure of graphite. This enhances the softness and self-lubricating property of the material. Based on the results, 0.8 nose radius insert tool exhibited good surface finish irrespective of composition and cutting parameters.

*3.6. Microtexture of Insert before and after Turning.* Figures 14(a), 14(b), 15(a), and 15(b) show the optical microtexture of carbide insert before and after turning of AA 7075-0% $TiB_2$ composite and AA 7075-3% $TiB_2$ of both with and without Gr in situ composite at highest cutting parameters. The optical inspection of flank face of the cutting inserts showed that more flank wear, nose deformation, and erosion of material over the tool occurred in the case of AA 7075-3% $TiB_2$ in situ composite when compared to AA 7075-3% $TiB_2$-1% Gr hybrid composite. The less damage of flank wear of tool was expected to be due to the presence of Gr particles which might have acted as good tribofilm surface between workpiece and tool.

## 4. Conclusions

The following conclusions can be drawn as the result of the experimental study of AA 7075/$x$% $TiB_2$/1% Gr and AA

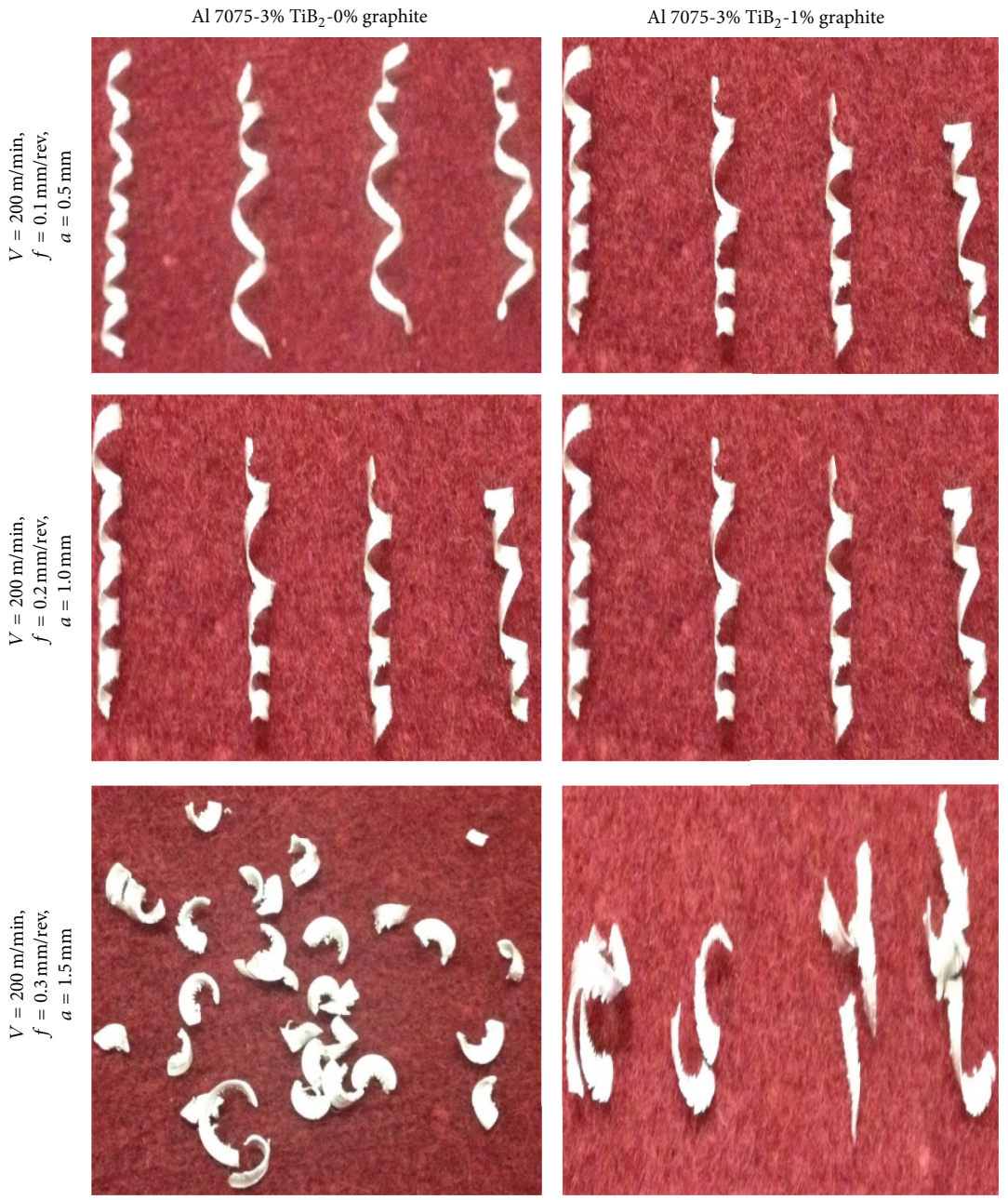


Figure 11: Examination of chip morphology with selected cutting parameters of AA 7075-3% $TiB_2$-0% Gr and AA 7075-3% $TiB_2$-1% Gr hybrid in situ composite with the cutting tool of 0.8 nose radius insert.

7075/3% $TiB_2$ in situ composite on mechanical and machining behavior:

(i) The XRD patterns of the prepared AMCs showed the formation of in situ $TiB_2$ particles without the presence of any other intermetallic compounds. Usually, it may occur during casting which can be identified via XRD. However, it was not observed. To ensure that, EDAX analysis was also performed (Figure 7(d)).

(ii) The flexural or bending stress, deflection, flexural or bending strain of AA 7075/$x$% $TiB_2$/1% Gr hybrid composite exhibited more value than AA 7075/3% $TiB_2$/0% Gr composite due to the presence of hard ceramic particles $TiB_2$ and graphite particles in the matrix.

(iii) The SEM micrograph shows a homogeneous distribution of $TiB_2$ particles and graphite particles in the aluminium matrix. The interface between the $TiB_2$, Gr particles, and matrix material was clean without the presence of pores and inclusions while comparing to the Al 7075/0% reinforcement material.

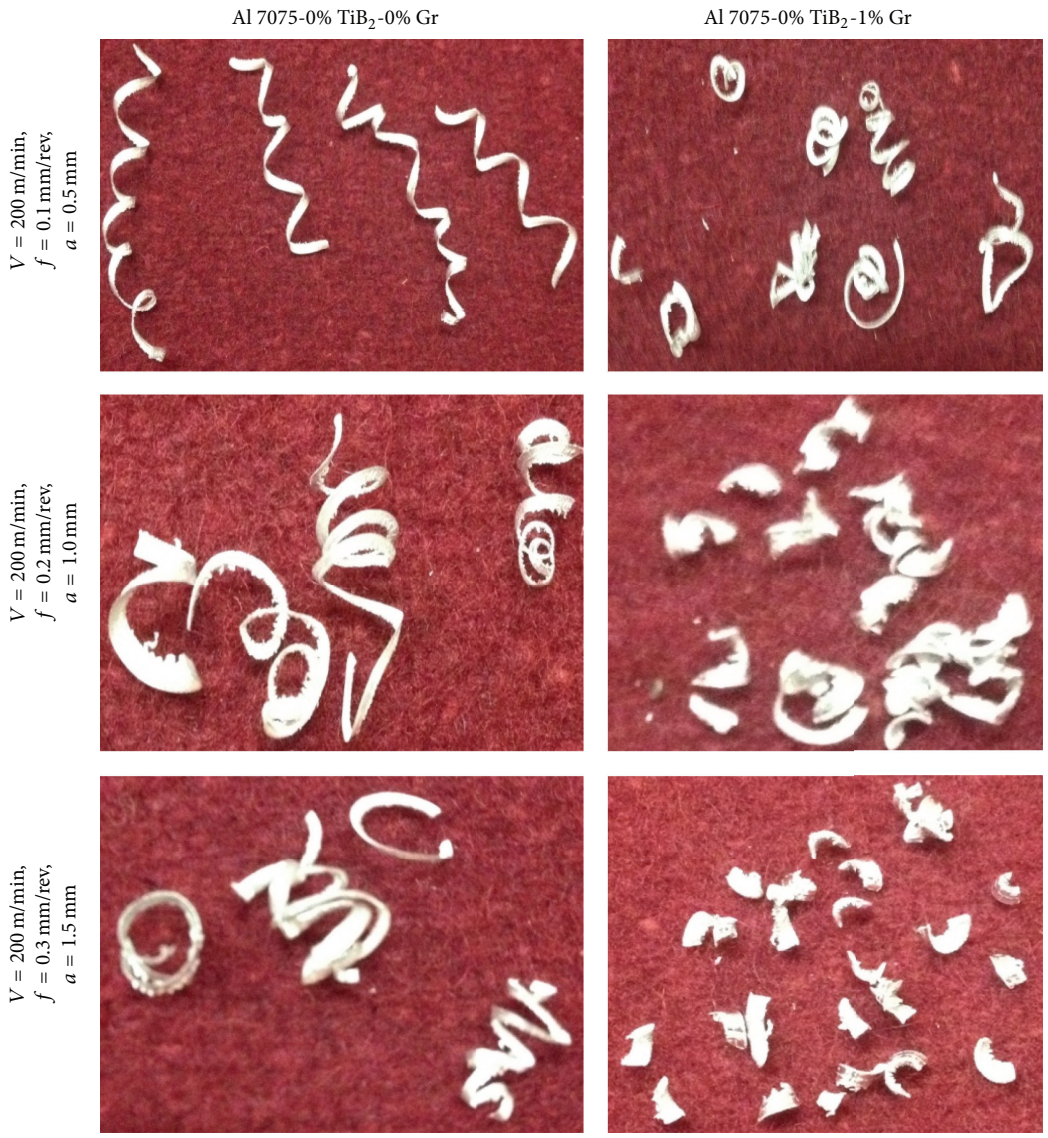


Figure 12: Examination of chip morphology with selected cutting parameters of Al 7075-3% $TiB_2$-0% Gr and Al 7075-3% $TiB_2$-1% Gr hybrid in situ composite with the cutting tool of 0.4 nose radius insert.

(iv) The SEM fractography images show that the larger amount of brittle nature contains Al 7075-6% $TiB_2$-1% Gr hybrid composite, due to larger amount of hard ceramic particles and 1% graphite particles present in Al 7075 matrix materials.

(v) The surface roughness value of AA 7075/$x$% $TiB_2$/1% Gr hybrid composite exhibited higher value with respect to higher spindle speed and feed rate when compared to AA 7075/3% $TiB_2$ composite and by using 0.8 mm nose radius insert exhibits good surface finish compared to the 0.4 mm nose radius insert. The optimum feed rate and depth of cut were observed as 0.1 mm/rev and 0.5 mm, where the surface roughness values were minimum at 0.8 mm nose radius insert.

(vi) Chip thickness increased when depth of cut and feed rate increased, and discontinuous chips formed as these parameters increased. While adding graphite to the metal matrix composite, more and more discontinuous chips formed. The size of these chips also decreased when the cutting speed, feed rate, and depth of cut increased.

(vii) Less tool damage was observed in 0.8 mm nose radius insert while turning of AA 7075-3% $TiB_2$-1% Gr hybrid in situ composite.

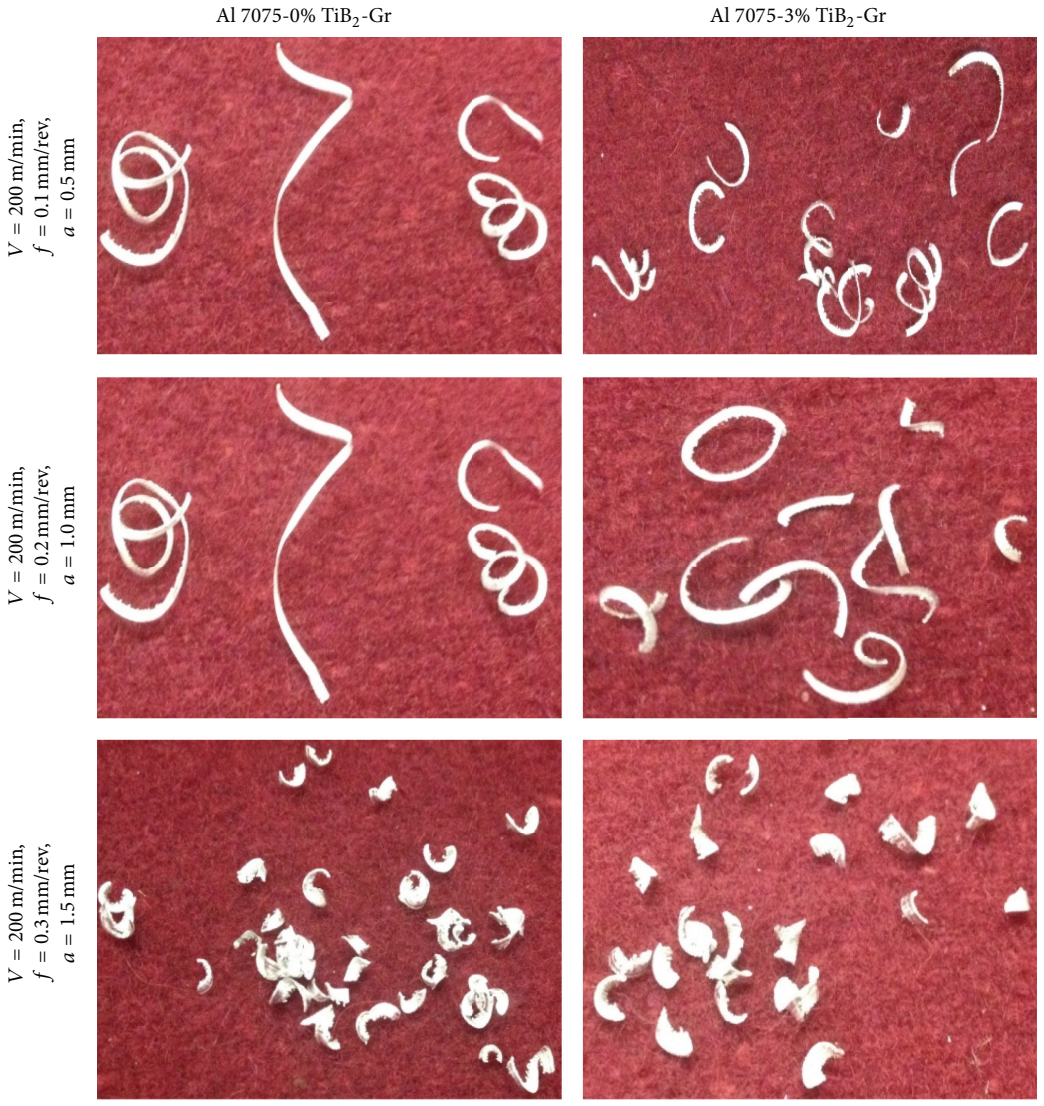


FIGURE 13: Examination of chip morphology with selected cutting parameters of Al 7075-3% $TiB_2$-0% Gr and Al 7075-3% $TiB_2$-1% Gr hybrid in situ composite with the cutting tool of 0.4 nose radius insert.

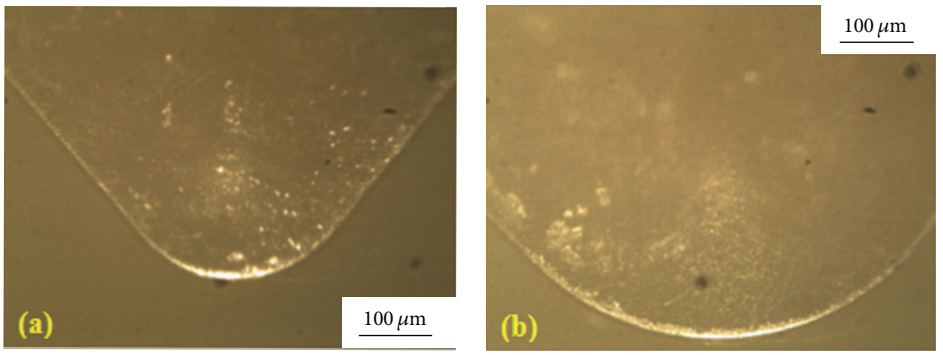


(a) (b)

FIGURE 14: Microtexture of insert before turning: (a) 0.4 mm nose radius and (b) 0.8 mm nose radius.

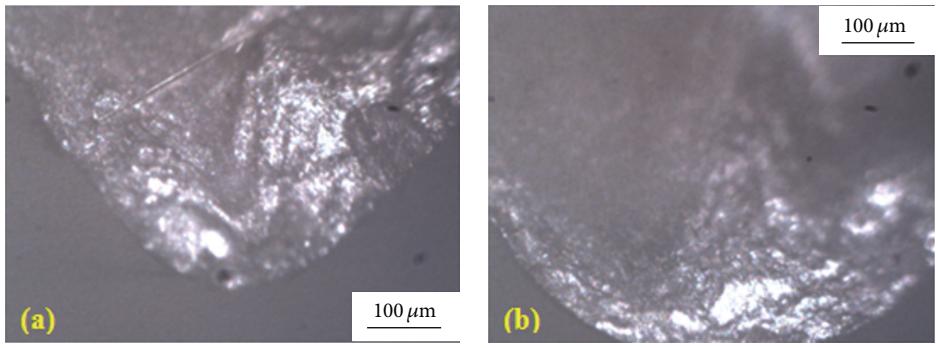


(a) (b)

Figure 15: Microtexture of insert after turning: (a) 0.4 mm nose radius and (b) 0.8 mm nose radius.

## Conflict of Interests

The authors declare that there is no conflict of interests regarding the publication of this paper.

## References

[1] B. Harris, *Engineering Composite Materials*, EPRI Center for Materials Production, 1999.

[2] T. W. Clyne, "Metal matrix composites: matrices and processing," in *Encyclopedia of Materials: Science and Technology*, p. 8, Elsevier, 2001.

[3] W. Hufenbach, H. Ullrich, M. Gude, A. Czulak, P. Malczyk, and V. Geske, "Manufacture studies and impact behaviour of light metal matrix composites reinforced by steel wires," *Archives of Civil and Mechanical Engineering*, vol. 12, no. 3, pp. 265–272, 2012.

[4] H. B. Michael Rajan, S. Ramabalan, I. Dinaharan, and S. J. Vijay, "Synthesis and characterization of in situ formed titanium diboride particulate reinforced AA7075 aluminum alloy cast composites," *Materials & Design*, vol. 44, pp. 438–445, 2013.

[5] G. Naveen Kumar, R. Narayanasamy, S. Natarajan, S. P. Kumaresh Babu, K. Sivaprasad, and S. Sivasankaran, "Dry sliding wear behaviour of AA 6351-ZrB2 in situ composite at room temperature," *Materials and Design*, vol. 31, no. 3, pp. 1526–1532, 2010.

[6] S. Kalpakjian and S. Schmid, *Manufacturing Processes for Engineering Materials*, Prentice Hall, 5th edition, 2007.

[7] K. Sivaprasad, S. P. K. Babu, S. Natarajan, R. Narayanasamy, B. A. Kumar, and G. Dinesh, "Study on abrasive and erosive wear behaviour of Al 6063/$TiB_2$ in situ composites," *Materials Science and Engineering A*, vol. 498, no. 1-2, pp. 495–500, 2008.

[8] R. K. Bhushan, S. Kumar, and S. Das, "Effect of machining parameters on surface roughness and tool wear for 7075 Al alloy SiC composite," *International Journal of Advanced Manufacturing Technology*, vol. 50, no. 5–8, pp. 459–469, 2010.

[9] K. Autar Kaw, *Mechanics of Composite Materials*, Taylor & Francis, 2nd edition, 2006.

[10] A. Baradeswaran and A. Elaya Perumal, "Study on mechanical and wear properties of Al 7075/$Al_2O_3$/graphite hybrid composites," *Composites Part B: Engineering*, vol. 56, pp. 464–471, 2014.

[11] N. B. Dhokey, S. Ghule, K. Rane, and R. S. Ranade, "Effect of KBF4 and K2TiF6 on precipitation kinetics of TiB2 in aluminium matrix composite," *Advanced Materials Letters*, vol. 2, no. 3, pp. 210–216, 2011.

[12] D. D. L. Chung, *Composite Materials: Functional Materials for Modern Technologies*, Springer, 2003.

[13] E. Kuram, B. Ozcelik, E. Demirbas, and E. Şık, "Effects of the cutting fluid types and cutting parameters on surface roughness and thrust force," in *Proceedings of the World Congress on Engineering (WCE '10)*, vol. 2, London, UK, June 2010.

[14] R. N. Rai, G. L. Datta, M. Chakraborty, and A. B. Chattopadhyay, "A study on the machinability behaviour of Al-TiC composite prepared by in situ technique," *Materials Science and Engineering A*, vol. 428, no. 1-2, pp. 34–40, 2006.